LAWRENCE
LIVERMORE
NATIONAL
LABORATORY

UCRL-JRNL-236360

Solvent-mediated repair and patterning of surfaces by AFM

S. Elhadj, A. Chernov, J. De Yoreo

November 8, 2007

Nanotechnology

Disclaimer

Solvent-mediated repair and patterning of surfaces by AFM

Selim Elhadj[†], *Alexander A. Chernov*[†], *James J. De Yoreo*[†]

[†] Department of Chemistry, Materials, Earth, and Life Sciences, Lawrence Livermore National Laboratory, 7000 East Avenue, Livermore, CA, 94550, USA

ABSTRACT

A tip-based approach to shaping surfaces of soluble materials with nanometer-scale control is reported. The proposed method can be used, for example, to eliminate defects and inhomogeneities in surface shape, repair mechanical or laser-induced damage to surfaces, or perform 3D lithography on the length scale of an AFM tip. The phenomenon that enables smoothing and repair of surfaces is based on the transport of material from regions of high- to low-curvature within the solution meniscus formed in a solvent-containing atmosphere between the surface in question and an AFM tip scanned over the surface. Using *in situ* AFM measurements of the kinetics of surface remodeling on KDP (KH_2PO_4) crystals in humid air, we show that redistribution of solute material during relaxation of grooves and mounds is driven by a reduction in surface free energy as described by the Gibbs-Thomson law. We find that the perturbation from a flat interface evolves according to the diffusion equation where the effective diffusivity is determined by the product of the surface stiffness and the step kinetic coefficient. We also show that, surprisingly, if the tip is instead scanned over or kept stationary above an atomically flat area of the surface, a convex structure is formed with a diameter that is controlled by the dimensions of the meniscus, indicating that the presence of the tip and meniscus reduces the substrate chemical

potential beneath that of the free surface. This allows one to create nanometer-scale 3D structures of arbitrary shape without the removal of substrate material or the use of extrinsic masks or chemical compounds. Potential applications of these tip-based phenomena are discussed.

KEYWORDS: patterning, repair, overgrowth, KDP, Gibbs-Thomson, humidity, solubility, AFM, stiffness, surface energy

Introduction. Since the discovery by Mirkin and co-workers[16, 27] that the meniscus formed through contact by an AFM tip with a solid substrate can be used as a vehicle for controlled deposition of self-assembled monolayers (SAMs) on Au, a wide variety of soluble molecules ranging in size from short alkyl thiols to DNA-oligomers have been used as "inks" to pattern Au and SiO_x substrates while achieving features as low as ~10nm[7, 16, 17, 22, 24]. The inks used in these patterns have often been designed to provide affinity templates for subsequent attachment of molecules or materials including proteins, antibodies, viruses, nanoparticles and nanowires[4, 5, 8, 18, 24, 37, 38, 41, 46, 47]. This constructive mode of lithography contrasts with most other patterning methods such as nano-grafting or imprint, e-beam and optical lithographies, which typically operate by removal of substrate material. But despite extensive research on numerous aspects of patterning through a tip-substrate meniscus, including the kinetics of tip-to-surface transport[26, 31, 33, 43], the dynamics of meniscus formation[44], multi-tip and multi-ink patterning[17], and assembly dynamics at affinity templates[4, 5, 42], no studies have been performed that explore the use of the meniscus itself as a tool for directly reconfiguring a surface with nanometer scale control.

The idea behind this approach is that the Kelvin effect[30] is used to form a meniscus at a tip-surface contact[44] where the meniscus is comprised of a solvent for that surface that is present in the surrounding atmosphere. By scanning this meniscus across the surface, the natural thermodynamic forces that drive transport of dissolved species and/or the elimination of curvature can be exploited to reconfigure the surface. In fact, here we show that this approach can be used either to eliminate defects in surfaces or to create arbitrary 3D nanometer scale patterns through tip-directed dissolution or overgrowth, respectively. The potential applications of this approach are far-reaching because most

materials are soluble to varying degrees in a range of solvents that can form a vapor near room temperature. For example, use of the meniscus to create static 3D structures too small to be detected on water-insoluble substrates could be used for encryption, while their formation on water-soluble materials would provide a tool for forensic analysis since the subsequent relaxation of these structures when the material has been tampered with (e.g., the packaging has been opened) would demark the time since their exposure to air. Conversely, use of the meniscus to eliminate deviations from surface flatness can be applied to the figuring of optical surfaces, elimination of surface defects and repair of mechanical and laser induced damage to surfaces. In essence, this probe-surface configuration constitutes the ultimate in small-tool figuring because the need for an extrinsic means for solvent delivery and removal as well as for controlling the area of solvent access are virtually eliminated, while the length scale of control is less than the wavelength of light.

Here we describe the results of an *in situ* AFM investigation into the kinetics of tip-based surface remodeling using KDP (KH_2PO_4) single crystals as the substrate and water as the solvent. We show that grooves (or mounds) fabricated on a KDP surface by and AFM tip relax away by in-filling (or dissolution) as the meniscus at the tip-substrate contact is scanned over the groove (or mound). We present a quantitative model for the redistribution of solute material during this process that is based on reduction of surface free energy and is in excellent agreement with the measurements. Because the observed tip-induced remodeling of the surface involves transport of solute species within an ultrathin aqueous layer adsorbed across the crystal surface in humid air, our results make contact with previous studies in which changes in surface morphology in air were found to occur on a broad range of alkali halide crystals surfaces [36, 45]. Even without tip perturbation, step edges on these crystal surfaces were shown to spontaneously change shape to minimize surface free energy[20] or, in some cases, to relieve strain [6, 21]. Although the kinetics of surface relaxation have been analyzed in detail at metal – vacuum and semiconductor – vacuum interfaces[15, 14, 19, 23], to the best of our knowledge, relaxation in solutions has not previously been investigated quantitatively, nor has the effect of a tip on the kinetics of this process been investigated.

We also present results on creation of arbitrary nanometer scale 3D structures through tip-induced overgrowth of the crystal within the region of the surface that lies below the meniscus. This also builds on previous observations in which material dissolved from the surface in the presence of a thin aqueous condensate layer was shown to re-deposit on the surface at the point of contact between the tip and the substrate. The simplest case reported was the drying of a solution droplet condensed between a surface and the AFM tip by capillarity action[44] after tip removal[32]. But more interesting, though not yet understood, was the re-deposition of crystal material in the area over which the tip-substrate meniscus was scanned in the absence of drying. This re-deposition was attributed to continuous evaporation of the meniscus[29, 34, 35], or even to differences in the water chemical potential in ultrathin water layers compared to bulk (i.e., within the meniscus)[13]. Although the physical mechanism that underlies this phenomenon still remains in question, here we use it to create 3D nanoscale structures and to study the kinetics of changes in surface shape when these overgrowths are allowed to relax away in order to minimize curvature and thus surface free energy.

Experimental. The material selected for study was KDP because it is extensively used in large-scale applications of non-linear optics such as frequency conversion and optical switching, which frequently suffer from laser-induced surface damage at high laser fluences. In this study, as the starting substrate we used the natural (100) vicinal faces of KDP, which have been extensively investigated and consist of a series of terraces separated by a combination of elementary steps and step bunches typically on the order of 10 steps in height. All data from this study were obtained on KDP (100) surfaces that were freshly etched by brief (~1 sec) exposure to filtered de-ionized H_2O and immediately dried with a jet of N_2 gas. This procedure was followed because we found that the ability of the surface to recover from a perturbation gradually decreased over time as the KDP surface was exposed to room air (see Supporting Information Fig. 3). Even without this precaution, under sufficient humidity (>35%), the perturbed surface always recovered and eventually returned to its original average vicinality.

The tip-based approach to the remodeling KDP surfaces is illustrated in **Fig. 1**. The entire AFM, including the sample, was placed in a Plexiglas chamber equipped with temperature and humidity

sensors (ets, Inc. model 554). Surface remodeling and imaging were performed at room temperature (ca. 20±2 °C) under a relative humidity (RH) that was set to a fixed value in the range of 35% to 95% (±5%) using a humidity controller and an ultrasonic humidifier (ets, Inc., PA, USA, model 5200). While the AFM tip was rastered over the surface, relaxation of both concave (**Fig. 1b**) and convex (**Fig. 1c**) deviations from the planar surface took place concomitantly with imaging using the same tip. In this way, we were able to obtain *in situ* images during the relaxation process. **Fig. 1a** gives a sequence of AFM images showing examples of the disappearance of a tip-made groove by in-filling as well as the simultaneous disappearance of a mound near the lower end of the groove by dissolution. A movie of this process can be found in the Supporting Information. The processes of groove healing and mound dissolution within the aqueous meniscus are also shown schematically in **Fig. 1b** and **c** respectively. The time evolution of the interface is depicted by labels "1 - 4" indicating successive stages of the process, beginning at "1".

To investigate the relaxation of concave features, grooves were made by mechanical etching with a stiff Si AFM tip (Nanoworld AG, Switzerland) using forces of 3,000-10,000 nN at the surface (**Fig. 1a**). The tip was moved along a single direction and location, back and forth, at 2Hz for ~10-20 sec to produce a groove 3 μm long, 50-1000 nm wide, and 10-250 nm deep, depending on the force and the etching time used. This procedure also gave us the opportunity to investigate relaxation of convex features since groove formation often resulted in the creation of a mound as seen in **Fig. 1a**. Although this method of making the groove caused a reduction in the sharpness of the tips, they remained usable for imaging over long periods of time, albeit with some loss in lateral resolution (see Supporting Information **Fig. 1**). However the resolution normal to the surface did not change, nor did our ability to image the entire surface of a groove since they had shallow sides with angles of less than ~20° relative to the average surface as compared to the steep ~75° angle of the AFM-tip edges with respect to the surface. Therefore, the ability of the tip to track depth, measure heights, and resolve relevant surface features remained unaffected following its use in making grooves.

We also investigated the growth and relaxation of convex structures on the surface (overgrowths) formed by keeping the tip stationary and in contact with the surface under 35-85% relative humidity for 1-60 minutes. The longer the time of contact the greater the height of the overgrowth (data not shown). Imaging of the surface was done over a 6x6 μm^2 area (512 x 512 lines) under constant force feedback mode using a force of 100-300 nN. (The force applied to the surface was estimated from the manufacturer's cantilever spring constant, which was nominally k_s = 42 nN/nm, and calibration of the diode-tip deflection sensitivity). All imaging was done in deflection mode (and height mode) so that the KDP step edges and step bunches appeared as bright or dark contour lines in the images. To collect an image, the tip was rastered perpendicular to the axis of the groove with a scan frequency of 2Hz and a linear tip velocity of 23.6 μm/sec. Hence, the complete capture of a single image took about 4 minutes. These imaging parameters were kept constant throughout the experiment.

The images were captured continuously during an experiment and later analyzed for changes in groove depth or mound height. Average groove depth was taken along the groove axis at the center where the bottom depth is also at a maximum relative to the original surface. The initial depth along the groove was relatively constant up until the groove ends. Mound height was measured as the height of the top surface of the mound relative to the substrate plane (100). The largest error in measuring the height and depth came from the uncertainty in the selection of the same "flat" reference surface outside of the feature being measured in each frame. This was compounded by the fact that the groove and mound shape changed over time and because the piezo stage of the AFM exhibited some drift.

Results

Measurements of surface remodeling kinetics. **Fig. 2** shows results obtained on the time dependence of relaxation at RH=85% for both a groove and a mound during continuous rastering of the tip. Although most of the measurements in this study were done at a RH of 55% and 85%, the results shown in **Fig. 2** are representative of measurements done at all RH above 35%. At RH levels of ~35% or less we found that the surface did not change on the time scale of the experiments. These low-

humidity experiments thus constituted a positive control experiment on the effect of the tip itself in the absence of solvent because, not only did the meniscus fail to form, but rastering the tip under our conditions of low applied force did not alter the surface over time. Rather, the groove depth and profile remained constant (for data at RH≤35%, see Supporting Information **Fig. 2**).

Separating the effects on recovery of the surface caused by tip rastering from that of the thin aqueous layer that forms independently of the tip was accomplished by performing rastering discontinuously. This allowed remodeling to take place in the absence of tip surface contact. Following collection of the initial image, subsequent images were captured at 20-30 minute intervals, during which time the tip was lifted well away from the surface. This procedure contrasted with the continuous rastering done during the tip-based remodeling protocol where the tip always remained in contact with the surface. Comparison of the rates obtained with the two methods is shown in **Fig. 3a**, where the rate of in-filling of the groove is seen to be substantially slower than that obtained with continuous rastering.

To confirm this tip enhancement effect, the tip was continuously rastered back-and forth normal to the groove axis at a single location along the length of a groove. Indeed, the cross-sectional profile along the length of the groove shows that much more material was deposited where the tip was rastering than elsewhere (**Fig. 3b**). The obvious relaxation of the surface in the absence of tip, shows that the underlying driving force is inherent to the surface-solvent system. But the enhancement of relaxation rates through continuous tip-rastering suggests one of two causes: 1) it forces faster solute transport either through direct mixing or advection driven by the dynamics of the meniscus-air interface, or 2) it creates a greater driving force (i.e., chemical potential gradient) for solute redistribution, perhaps through the effect of solvent layer thickness on solubility. These possibilities will be further discussed below.

3D patterning by tip-driven overgrowth. In contrast to in-filling of a groove, the images in **Fig. 4a** demonstrate the spontaneous creation of a cylindrical mound or "dot" due to material deposition under an immobile tip touching an arbitrary site on the original vicinal surface. During the formation of each dot, the tip was kept in contact for the same amount of time (~17 min) at the humidity levels indicated. The mound size thus increases with both time of contact (data not shown) and relative humidity (**Fig.**

4a). Our measurements of dot size are consistent with the dependence of meniscus size on humidity determined previously with silicon nitride tips on Si substrates using *in situ* E-SEM measurements [44]. Thus we conclude that the size of the overgrowth corresponds to the "footprint" of the meniscus on the substrate. This provides a means to control the size of features created through this method of patterning.

Removal of the tip from these overgrowths results in their spontaneous relaxation back to the initial vicinal surface. As the *in situ* images of this process show (**Fig. 4b** and movie in Supporting Information), the onset of relaxation occurs spontaneously after the tip is lifted from the surface and proceeds through layer-by-layer dissolution of steps that are ~0.4 nm in height, a value expected for elementary steps based on the lattice parameter perpendicular to the KDP (100) face[28]. Initially, as each new layer dissolves, the newly exposed layer becomes a shrinking 2D island. The driving force for this process will be discussed later, but the implication of these results is that the mechanism of growth includes layer-by-layer nucleation of islands on top of the original vicinal surface within the tip-substrate meniscus. The presence of 2D islands indicates that the supersaturation within the meniscus during the formation of the overgrowth was significant. We estimate this supersaturation to have been at least 10%[9]. As soon as all the 2D islands on the overgrowth were dissolved, only the steps on the original vicinal surface remained. These steps, which grew within the boundaries of the meniscus, had tongue-like protrusions that formed during the overgrowth formation and pointed down the vicinal surface. As each tongue retreated, the original straight steps on the vicinal face were restored (see **Fig. 4b** and movie in Supporting Information).

Taking advantage of this phenomenon of tip-induced overgrowth, we were able to create a line of overgrown material by rastering the tip and meniscus along a single direction, (**Fig. 4c**). As with the dot diameter, the width of this line is determined by the size of the meniscus, which, in turn, depends on the level of humidity (**Fig. 3**), the tip chemistry (wetting of surface), and the size of the tip itself. The length and shape of the line formed can be arbitrarily determined because they only depend on the pattern followed in rastering the tip over the surface. To the best of our knowledge, this is the first

demonstration of a constructive method for making an arbitrary nanometer-scale 3D pattern on a substrate using the native substrate material.

Mechanism of solute transport in thin aqueous solvent. Fig. 5 shows that a plot of overgrowth height versus the inverse of the meniscus diameter as determined from the overgrowth diameter gives a linear relationship over the range of RH from 55% to 85%, while between 85% and 95% there is a sharp increase in the strength of this dependence. A simple mass balance calculation shows that this result implies that the thin aqueous film covering the crystal surface through which solute molecules are transported to the region of overgrowth is of nearly constant thickness over the RH range of 55-85%. To account for the rate of overgrowth, the mass current through the cross-section of the film around the overgrowth must be equal to $\rho(dV/dt)=\rho A(dZ/dt) = \rho\pi R^2(dZ/dt)$ where ρ is the solid density, V is the overgrown volume, Z is the height of the overgrowth, A is its area and R is its radius. This current must be equal to $2\pi R\delta\Phi$, where R is the radius of the meniscus, δ is the thickness of the aqueous layer away from the overgrowth, and Φ flux (mass transported per unit area per unit time) into the meniscus. Thus, taking the area A— and therefore R — to be a constant of time determined by the meniscus size (i.e., the humidity), at fixed time t, $Z \sim R^{-1}$ if $\delta\Phi$ is a constant. Using overgrowth height measurements shown, in part, in **Fig. 4a**, we find that the plot of the overgrowth height versus the inverse of the meniscus diameter is indeed linear between RH of 55% and 85%. Since Φ is only dependent on the concentration gradient, which will not depend on R, the implication is that, between 55% and 85% RH, the aqueous film thickness δ is roughly constant. The stronger dependence above 85% indicates that the aqueous film thickens at these higher humidity levels.

The tendency for the aqueous film thickness to remain nearly unchanged in the 55-85% range of humidity is consistent with the findings of previous studies [10]. Moreover, in our own measurements (data not shown) of the aqueous layer thickness, δ(RH), by distance dynamic force spectroscopy [25], we found that $\delta(35\%) \sim 0.3$ nm corresponding to a monolayer-to-submonolayer regime, while for RH of 45% and 55%, the layer thickness remained constant at $\delta = 0.8$ nm, consistent with about two monolayers of water on the surface. Our observations are also consistent with E-SEM measurements of

water film thickness on Si[44], and FT-IR measurements of Langmuir water adsorption isotherms on MgO (100) surfaces[11] and NaCl (001) surfaces[12]. The latter film measurements all showed a highly nonlinear increase in water thickness and coverage for RH > 80%. Therefore we conclude that 1) surface remodeling depends on the formation of an aqueous solvent layer and, 2) this layer must be greater than a monolayer in thickness either to be able to solvate the solute molecules [40] or to allow transport over the surface, or both since, as already stated, no surface changes are observed at humidity levels of 35% or less where a submonolayer water regime prevails.

Discussion

Driving force for surface healing and kinetic data analysis. Spontaneous elimination of grooves and mounds suggest that these processes are driven by minimization of the crystal-solution surface free energy, i.e. through the Gibbs-Thomson effect. To outline the equations governing surface shape evolution in two dimensions, consider the perturbed interface profile Z = Z(x,t) at time t containing the groove normal to x and parallel to the y axis on the originally flat interface Z(x,y) = 0 (**Fig. 1**). The groove walls are built of intensively fluctuating steps typical of KDP faces. Therefore the growth rate of the wall normal to itself, V is derived here and is given by,

$$V = \omega\beta\{C - C_{e0}[1-(\omega\tilde{\alpha}/kT)Z''(x,t)/(1+Z'^2)^{3/2}]\} \qquad \textbf{(1)}$$

and should be linear with respect to local supersaturation, C-C_e, where C(x,y,t) is the actual and C_e is the equilibrium solution concentration at the wall. The latter concentration should be corrected for the wall curvature, which contributes to the supersaturation according to the Gibbs-Thomson law. The KDP wall growth kinetic coefficient, β, is proportional to the local wall slope $p(x) \equiv \tan\theta = \partial Z/\partial x \equiv Z'$. The wall kinetic coefficient $\beta=\beta_{st}p$, with β_{st} standing for the similarly defined step kinetic coefficient. At room temperature on the (100) face, $\beta_{st} = 7\text{x}10^{-2}$ cm/s[28]. The $\omega = 10^{-22}$ cm^3 in **eq.(1)** designates the specific molecular volume of the solid, $\tilde{\alpha} = \alpha+\partial^2\alpha/\partial\theta^2$, where $\tilde{\alpha}$ and α represent the surface stiffness and surface free energy, respectively, kT is the thermal energy and the primes at Z(x,t) mean derivatives with respect to x. Surface energy decreases when the concave bottom of the groove is being filled with

the material dissolving at the convex groove shoulders. The rate of the wall propagation in the z-direction is given by:

$$\partial Z/\partial t = V\sqrt{(1+p^2)}. \qquad \textbf{(2)}$$

Substituting **eq.(1)** into **eq.(2)** we obtain a differential equation for the groove profile $Z = Z(x,t)$. The initial condition for this equation is $Z(x,0) = Z_0(x)$, representing the initial groove shape at $t = 0$. As $x \to \infty$, $Z \to 0$. **Eq.(2)** is non linear since β and $\tilde{\alpha} = \alpha+\partial^2\alpha/\partial\theta^2$ depend on the wall slope, $\partial Z/\partial x$. Also, generally speaking, $C = C(x,t)$ and obeys the mass transport equations in the solution filling the groove. Moreover, the groove wall evolves in time.

Having in mind the experimental accuracy achieved, we shall now simplify the problem down to a level that allows an adequate approximate analytical solution. Major shape changes occur within an hour when the wall slope decreases 2-3 times from the initial average slope $p \approx 0.3$ (**Fig. 2a**). Thus we may ignore Z'^2 as compared with unity in **eq.(1)**. Also, taking arbitrarily the time average of the slope to be $p_0 = 0.25$ ($\theta = 14°$) we can take the wall kinetic coefficient as independent of the slope, with a value $\beta = 1.8\text{x}10^{-2}$ cm/s[28], which applies for both growth and dissolution. In a stagnant droplet of the size $L \approx 1$mkm and with solute molecular diffusivity $D_m \approx 10^{-5}$ cm^2/s[28], the typical diffusion rate is $D_m/L \approx 0.1$cm/s $> \beta \sim 2\text{x}10^{-2}$cm/s. Mixing in a scanning droplet replaces the molecular diffusivity by a larger convective diffusivity and thus enhances this inequality. **Fig. 3 a** and **b** comparing healing rate with and without droplet motion over the surface qualitatively supports this conclusion. Therefore the mass transport and thus the groove healing rate may be taken as controlled by the interface growth and dissolution kinetics. Consequently, we assume the concentration to be equal to its value over the flat interface, $C = C_{e0}$, which is the average between the convex and concave portions of the groove wall and is also achieved when the scanning droplet is in contact with the flat interface. Overgrowth of the surface under a moving and still tip suggests that a supersaturation exists in the droplet. However, the deposition rate is low as compared to the healing rate. Also addition of the term linear in time to the solution **eq.(4)** below does not change results noticeably. Therefore we still keep $C=C_{e0}$, the assumption

that decouples the groove shape from solute distribution within the groove. Thus, the approximations mentioned above maps the groove shape problem to the simple diffusion equation:

$$\partial Z/\partial t = D_s \partial^2 Z/\partial x^2, \text{ where } D_s \equiv \omega 2 C_{e0} \tilde{\alpha} \beta/kT \qquad \textbf{(3)}$$

In this equation the effective diffusivity D_s is controlled by the surface kinetic coefficient and stiffness and has nothing to do with the real molecular diffusivity, D_m. The **eq.(3)** means simply that the groove profile should evolve in time just as it would for an initial two dimensional concentration distribution Z = Z(x,0) in an infinite solution with the effective diffusivity D_s. For a perturbation on a step, a similar mapping was made, e.g., in studies by Burton *et al*[2] .

For the initial groove of symmetric triangular cross section with the depth Z_0 and the base $2x_0$ long, the solution of **eq.(3)** is:

$$Z(0,t)/Z_0 = \text{erf}(x_0/2\sqrt{(D_s t)}) + [2\sqrt{(D_s t)}/\sqrt{\pi} x_0][\exp(-x_0^2/4D_s t) - 1] \qquad \textbf{(4)}$$

The equation for the evolution of a cylindrical overgrowth is similar to **eq.(3)** for the groove evolution although its solution requires 3 dimensions. Within the same approximations of a small and constant wall slope, the only difference is that the Gibbs-Thomson shift of the chemical potential comprising deviation from unity in the square bracket term in **eq.(1)** is now proportional to $(\alpha + \partial^2\alpha/\partial\theta_x^{\,2})\partial^2 z/\partial x^2 + (\alpha + \partial^2\alpha/\partial\theta_y^{\,2})\partial^2 z/\partial y^2$ instead of $\tilde{\alpha}\,\partial^2 z/\partial x^2$ as in **eq.(1)**. Here y is the axis normal to the x axis in the unperturbed plane z = 0 normal to the x axis, while $\theta_x \equiv \theta$ and θ_y is the surface slope angle with respect to the y axis. Assuming the stiffness relative to the y-axis to be equal to that relative to the x-axis we arrive, in place of **eq.(1)** at:

$$\partial Z/\partial t = D_s(\partial^2 Z/\partial x^2 + \partial^2 Z/\partial y^2) \qquad \textbf{(5)}$$

If the initial overgrowth shape is a truncated circular pyramid of height Z_0 with the upper and lower radii x_0 and r_1 then the pyramid height changes with time as:

$$Z(0,t)/Z_0 = 1 - [\sqrt{(\pi D_s t)}/(r_1 - r_0)][\text{erf}(r_1/2\sqrt{(D_s t)}) - \text{erf}(r_0/2\sqrt{(D_s t)})] \qquad \textbf{(6)}$$

If the initial overgrowth shape is just a cylinder of radius r_0 then, from **eq.(6)** or directly from the diffusion equation, the solution is even simpler:

$$Z(0,t)/Z_0 = 1 - \exp(-r_0^2/4D_s t) \quad \textbf{(7)}$$

However fitting of our data is improved when **eq.(6)** is used instead of **eq.(7)**, not unexpectedly, since from AFM images the initial shape of the overgrowth more closely resembled a circular pyramid than a cylinder. Therefore fitting the original experimental data for the groove (**eq.(4)**), as in **Fig. 2** for example, with the actual measured r_0 and Z_0 and performing a similar fitting of the data for the overgrowth (**eq.(6)**) yields the effective diffusivities, D_s, for the fittings that are summarized in **Table 1**.

Thus for 55% humidity, groove healing corresponds to $D_s = 9.0\text{x}10^{-12}$ cm^2/s. Then, taking T = 298K, $\omega = 10^{-22}$ cm^3, $\omega C_{e0} = 0.066$, $\beta = 1.8\text{x}10^{-2}$ cm/s[28,] we obtain $\tilde{\alpha}$ = 3.1 erg/cm^2 ($\tilde{\alpha}$ = 6.5 erg/cm^2, at 85% RH). From the overgrowth data at 55% humidity, $D_s = 3.3\text{x}10^{-11}$ cm^2/s and $\tilde{\alpha}$ = 11.2 erg/cm^2 ($\tilde{\alpha}$ = 5.8 erg/cm^2, at 85% RH). The experimentally measured step free energy per unit step height on KDP is ~ 20 erg/cm^2[28], i.e. it is substantially larger. If the values extracted from the model can be trusted, this inequality between the surface energy and stiffness suggests that the second derivative $\partial^2\alpha/\partial\theta^2$ in the surface stiffness for KDP (100) is larger than α as is the case, for example, with the weakly anisotropic surface energy of succinonitrile in its melt[1]. The surface stiffness is known to be the measure of the step-step interactions[39]. Indeed, the stiffness is zero for any stepped surface deviated from the nearest singular close packed orientation by angle θ - if its free energy taken just as a sum $\alpha = \alpha_t\cos\theta + \alpha_s\sin\theta$ of additive contributions from terraces (term with α_t) and steps (term with α_s). The contribution to the stiffness from mutual entropy repulsion between steps is ~ $(kT)^2\theta\ln 2/(2\tilde{\alpha}_{st}\, h^3)$ where $\tilde{\alpha}_{st}$ (erg/cm^2) stands for the step stiffness[3]. For the rather rounded steps that make up an overgrowth (**Fig. 2c**), we may expect the step riser stiffness to be equal to the step riser energy, ~20erg/cm^2. With this, the above estimate results in a stiffness of ~0.2 erg/cm2, an order of magnitude less than what is expected from the experimental results presented here. This discrepancy might come from development of a singular face on the bottom of the grove and top of the mound to which the isotropic model used above without adjustable parameters is poorly applicable. Then the parameter of the stiffness may

reflect the rate at which the steps are emanating from the groove or the overgrowth walls to propagate over the singular face. Thus, so far, the stiffness may be considered as an effective parameter. There might be also additional mechanisms for the mutual repulsion between steps, which are yet to be determined.

Leveling of grooves and mounds, both made by AFM tip, may be described as a result of the free surface energy minimization. The groove or mound overgrowth depth profile evolution can be mapped over to the diffusion equation with effective diffusivity proportional to the interface stiffness and kinetic coefficient. This mapping allows us to experimentally estimate, for the first time, the surface stiffness, i.e. the interaction between steps in solution. The healing of grooves and mounds and ability to deposit material under the AFM tip opens the way to patterning and repair of soluble surfaces at room temperature. The phenomenon of meniscus deposition and patterning of native material is still unresolved. The problem is likely related to the air/solvent dynamics at the interface or, possibly, to changes in the chemical potential and water structuring resulting from confinement within ultrathin solvent layers on surfaces.

Acknowledgements

We acknowledge the support of the U.S. Department of Energy, Office of Basic Energy Science, Division of Materials Science and Engineering as well as the Lawrence Livermore National Laboratory Research and Development Program. Prepared by LLNL under Contract DE-AC52-07NA27344.

Figure Captions

Figure 1. (a) AFM deflection images sequence of the in-filling of the groove made by tip scratching on a KDP (100) surface. The KDP material excavated during the scratching was re-deposited at the lower end of the groove on the image and dissolves over time. This surface remodeling occurs in a humid air environment which produces an aqueous meniscus as depicted in the (b) schematic of the time evolution

of the in-filling of the groove (1-4), and in the (c) schematic of the evolution of the dissolution of the mound (1-4).

Figure 2. (a) Evolution of the groove cross-section on a KDP surface from AFM images of the surface topography when continuously rastering with and AFM tip over the surface in a humid air environment (85% RH). (b) AFM measurements of the depth of the groove are plotted as a function of time normalized by the initial depth of the groove. The fitting of the data (see text for details) is indicated by the solid line. (c) A KDP mound was formed by keeping a stationary tip in contact with the KDP surface as described in the text. Evolution of the mound cross-section is obtained from AFM images captured sequentially in a humid air environment (85% RH). AFM measurements of the height of the mound are plotted as a function of time normalized by the initial height of the groove. The fitting of the data (see text for details) is indicated by the solid line.

Figure 3. (a) Comparison of the dynamics of the change of the groove depth in a humid air environment (85% RH) with the AFM tip continuously rastering the KDP surface (red curve) and intermittent rastering (blue curve). During continuous rastering the tip is in constant contact with the KDP surface, while during the intermittent rastering the tip remains away from the surface (for 24 minutes) between the times of rastering and depth measurement. The depth measurements shown are normalized to the initial groove depth. (b) When the tip is rastered perpendicular to the groove axis continuously back and forth at 85% RH, the cross-section along the groove shows a bump or material re-deposited where the rastering occurred at the location depicted by the deflection AFM image.

Figure 4. (a) AFM deflection images of the KDP mounds of the overgrown surface for increasing levels of relative humidity (65%-95% RH). The mounds were produced as described in the text by stationary contact with an AFM tip for a fixed amount of time of 17 minutes in a humid air environment. (b) The dissolution of the mound occurs spontaneously after the tip is moved away as

shown by the sequence of AFM deflection images. This dissolution process of the KDP mound involves the dissolution, initially, of 2D islands and then sequential step retreat. (c) The material can also be overgrown in any arbitrary shape by, for ex., scanning the tip back and forth along a single direction to form an overgrowth line (image size is 6 6 μm^2).

Figure 5. AFM measurements of the dependence of the KDP overgrowth mound height on the inverse of the meniscus diameter for the relative air humidity levels indicated. The meniscus diameters were determined from the size of the overgrown footprint (**Fig. 4**) as explained in the text.

Table 1. Comparison of the effective diffusivity (**eq.(3)**), D_s, of the boundary of the KDP surface obtained by fitting groove depth and mound height data (**Fig. 2**), with the independently estimated calculated D_s (**eq.(3)**) from literature values of its constituents parameters . This diffusivity is related to the rate of change in the shape of the surface following a perturbation as, for ex., a scratch on a surface (see text for details), rather than the conventional molecular diffusivity of solutes.

	Experimental D_s* (cm^2/sec)		Estimated D_s (cm^2/sec)
	groove	mound overgrowth	
55% RH	$9.0\ 10^{-12} \pm 6.2\ 10^{-12}$	$3.3\ 10^{-11} \pm 1.3\ 10^{-11}$	$2.0\ 10^{-11}$
85% RH	$1.9\ 10^{-11} \pm 1.4\ 10^{-11}$	$1.7\ 10^{-11} \pm 1.3\ 10^{-11}$	

*values are means ± standard deviation. For 55% RH, n=7 independent experiments for groove experiments and n=5 for overgrowth experiments. For 85% RH, n=8 for groove experiments and n=5 for overgrowth experiments. D_s values are the same within experimental variability ($p>0.05$) except between groove and overgrowth D_s means at 55% rh ($p=0.014$).

FIGURES

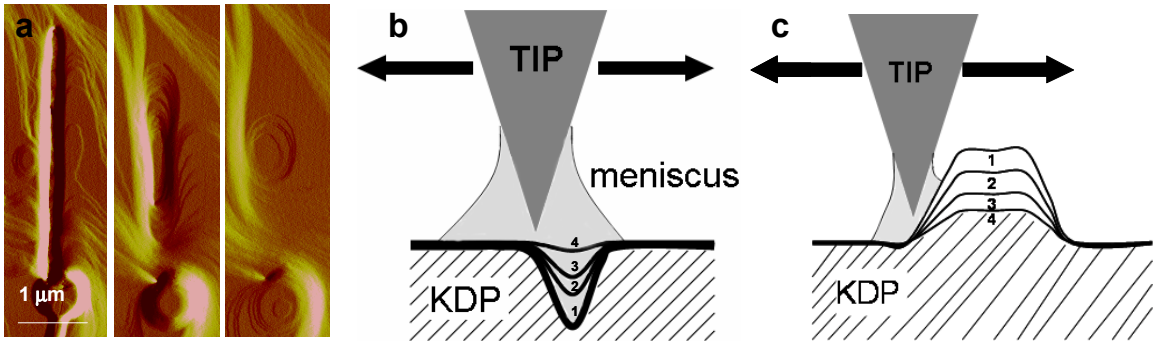

Figure. 1.

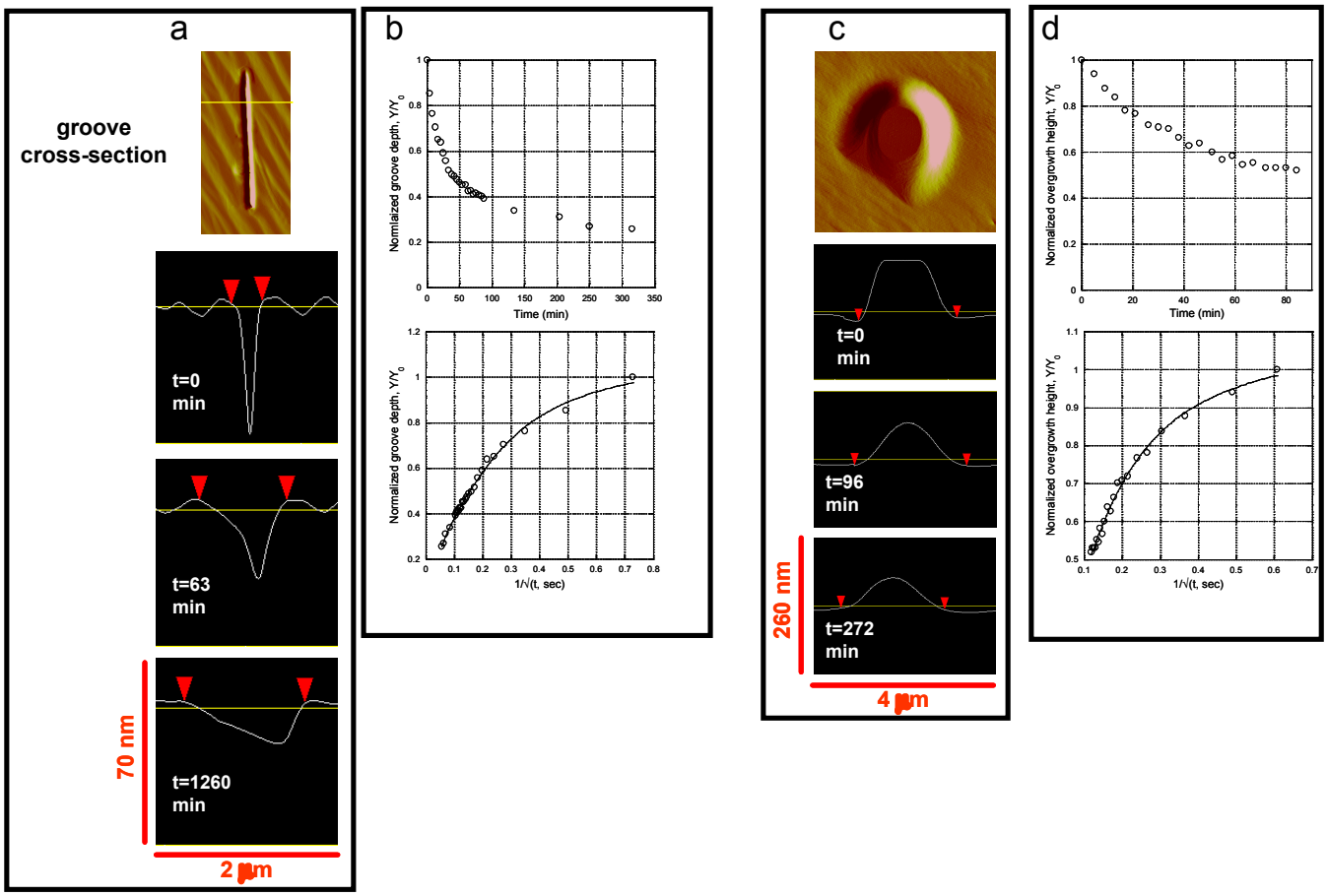

Figure.2.

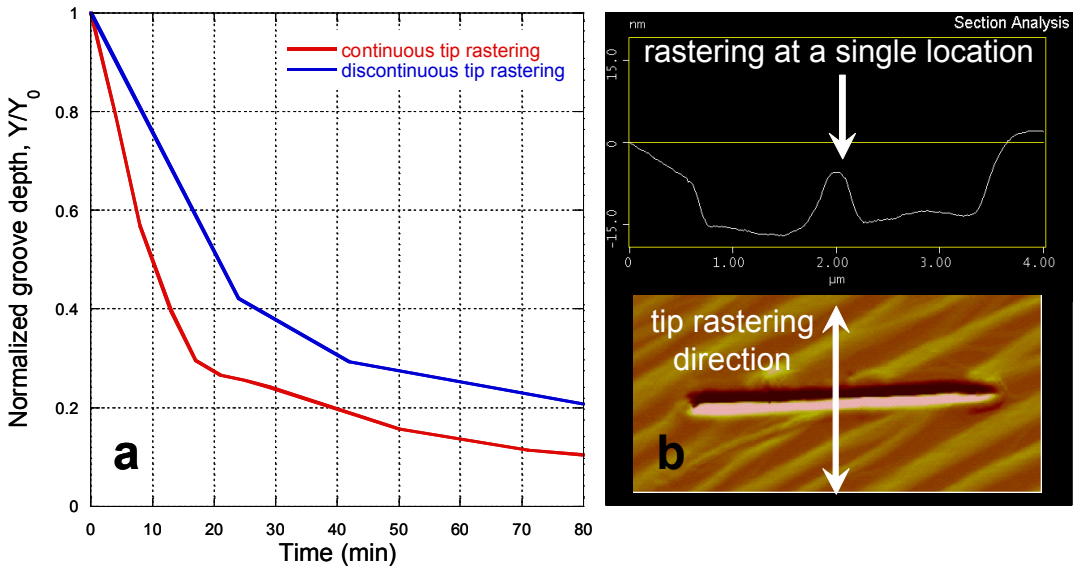

Figure. 3.

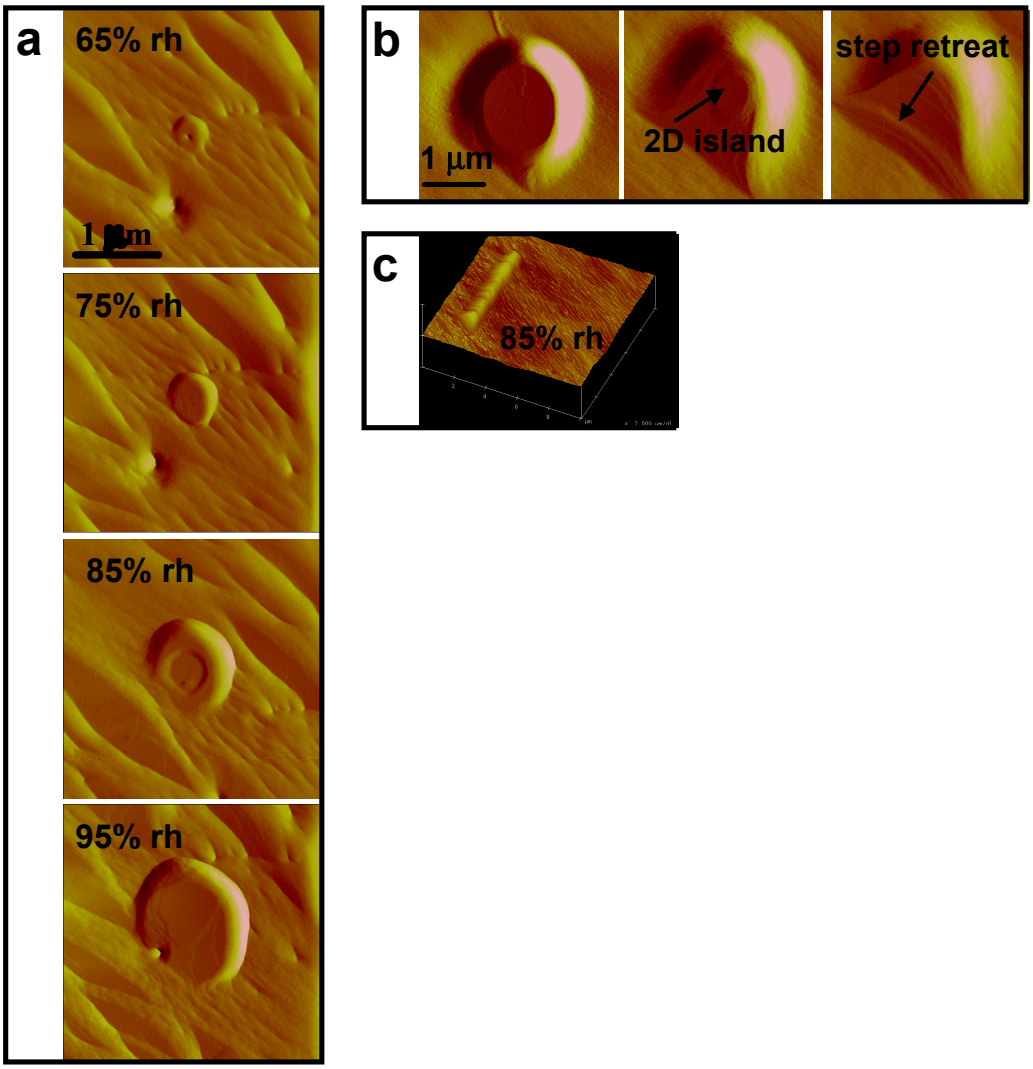

Figure. 4.

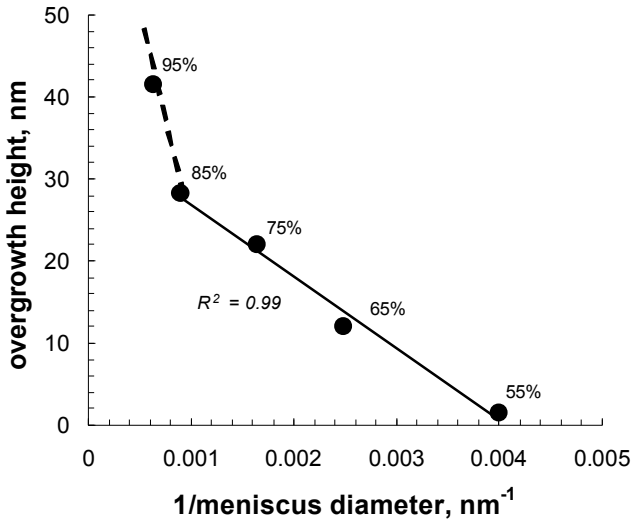

Figure. 5.

SUPPORTING INFORMATION AVAILABLE

1 AFM movie of the groove disappearing in humid air

1 AFM movie of the mound overgrowth disappearing in humid air

Figure 1. SEM images of the AFM tip before and after use for imaging and scratching the surface

Figure 2. Groove depth AFM measurements of the rate of the groove in-filling recovery in 35% vs 85% relative humidity.

Figure 3. Groove depth AFM measurements describing the reduction in the ability of the groove to recover over time depending on the amount of time the KDP surface was exposed to ambient air before and after water etching step of the surface as described in the text.

References

[1] Borzsonyi T, Buka A and Kramer L 1998 *Physical Review E* **58** 6236-45
[2] Burton W K, Cabrera N and Frank F C 1951 *Phil. Trans. R. Soc. Lond. A* **243** 299-358
[3] Chernov A A 1998 *Mater Sci Forum* **276-2** 57-69
[4] Cheung C L, Camarero J A, Woods B W, Lin T W, Johnson J E and De Yoreo J J 2003 *J Am Chem Soc* **125** 6848-9
[5] Cheung C L, Chung S W, Chatterji A, Lin T W, Johnson J E, Hok S, Perkins J and De Yoreo J J 2006 *J Am Chem Soc* **128** 10801-7
[6] Dai Q, Hu J and Salmeron M 1997 *J Phys Chem B* **101** 1994-8
[7] Demers L M, Ginger D S, Park S J, Li Z, Chung S W and Mirkin C A 2002 *Science* **296** 1836-8
[8] Demers L M and Mirkin C A 2001 *Angew Chem Int Edit* **40** 3069-71
[9] Deyoreo J J, Land T A and Dair B 1994 *Phys Rev Lett* **73** 838-41
[10] Ewing G E 2006 *Chemical Reviews* **106** 1511-26
[11] Foster M, D'Agostino M and Passno D 2005 *Surf Sci* **590** 31-41
[12] Foster M C and Ewing G E 2000 *J Chem Phys* **112** 6817-26
[13] Garcia-Manyes S, Verdaguer A, Gorostiza P and Sanz F 2004 *J Chem Phys* **120** 2963-71
[14] Giesen M 2001 *Progress in Surface Science* **68** 1-153
[15] Giesen M 2007 An atomic view on fundamental transport processes on metal surfaces. In: *AIP Conference Proceedings 916,* ed J Skowrongski*, et al.* (New York: Melville) pp 115-35
[16] Ginger D S, Zhang H and Mirkin C A 2004 *Angew Chem Int Edit* **43** 30-45
[17] Hong S H, Zhu J and Mirkin C A 1999 *Science* **286** 523-5
[18] Ivanisevic A, Im J H, Lee K B, Park S J, Demers L M, Watson K J and Mirkin C A 2001 *J Am Chem Soc* **123** 12424-5
[19] Jeong H C and Williams E D 1999 *Surface Science Reports* **34** 171-294
[20] Keller K W 1974 Crystal Growth and Characterization. In: *Proceedings of the ISSCG2 Spring School,* ed R Ueda and J B Mullin (Japan: North-Holland Publishin Company)
[21] Luna M, Rieutord F, Melman N A, Dai Q and Salmeron M 1998 *Journal of Physical Chemistry A* **102** 6793-800
[22] Maynor B W, Filocamo S F, Grinstaff M W and Liu J 2002 *J Am Chem Soc* **124** 522-3
[23] Mullins W W 1959 *J Appl Phys* **30** 77-83
[24] Noy A, Miller A E, Klare J E, Weeks B L, Woods B W and DeYoreo J J 2002 *Nano Lett* **2** 109-12
[25] Opitz A, Scherge M, Ahmed S I U and Schaefer J A 2007 *J Appl Phys* **101** -
[26] Peterson E J, Weeks B L, De Yoreo J J and Schwartz P V 2004 *J Phys Chem B* **108** 15206-10
[27] Piner R D, Zhu J, Xu F, Hong S H and Mirkin C A 1999 *Science* **283** 661-3
[28] Rashkovich L N 1991 *KDP - Family Single Crystals* (New York: Adam Hilger)
[29] Rashkovich L N, Shustin O A and Chernevich T G 1999 *J Cryst Growth* **206** 252-4
[30] Rief F 1965 *Fundamentals of Statistical and Thermal Physics* (San Francisco: McGraw-Hill)
[31] Rozhok S, Piner R and Mirkin C A 2003 *J Phys Chem B* **107** 751-7
[32] Rozhok S, Sun P, Piner R, Lieberman M and Mirkin C A 2004 *J Phys Chem B* **108** 7814-9
[33] Sheehan P E and Whitman L J 2002 *Phys Rev Lett* **88** -
[34] Shindo H, Ohashi M, Baba K and Seo A 1996 *Surf Sci* **358** 111-4
[35] Shindo H, Ohashi M, Tateishi O and Seo A 1997 *Journal of the Chemical Society-Faraday Transactions* **93** 1169-74
[36] Shluger A L, Wilson R M and Williams R T 1994 *Physical Review B* **49** 4915-30
[37] Vega R A, Maspoch D, Salaita K and Mirkin C A 2005 *Angew Chem Int Edit* **44** 6013-5
[38] Vega R A, Shen C K F, Maspoch D, Robach J G, Lamb R A and Mirkin C A 2007 *Small* **3** 1482-5
[39] Vekilov P G, Kuznetsov Y G and Chernov A A 1992 *J Cryst Growth* **121** 643-55
[40] Verdaguer A, Sacha G M, Bluhm H and Salmeron M 2006 *Chemical Reviews* **106** 1478-510
[41] Wang Y H, Maspoch D, Zou S L, Schatz G C, Smalley R E and Mirkin C A 2006 *P Natl Acad Sci USA* **103** 2026-31

[42] Weeks B, Cheung C L and De Yoreo J J 2004 *Assembly in Hybrid and Biological Systems* vol 2 (New York: Kluewer Academic Publishers)
[43] Weeks B L, Noy A, Miller A E and De Yoreo J J 2002 *Phys Rev Lett* **88** -
[44] Weeks B L, Vaughn M W and DeYoreo J J 2005 *Langmuir* **21** 8096-8
[45] Williams R T, Wilson R M and Liu H L 1992 *Nuclear Instruments & Methods in Physics Research Section B-Beam Interactions with Materials and Atoms* **65** 473-83
[46] Wilson D L, Martin R, Hong S, Cronin-Golomb M, Mirkin C A and Kaplan D L 2001 *P Natl Acad Sci USA* **98** 13660-4
[47] Zou S L, Maspoch D, Wang Y H, Mirkin C A and Schatz G C 2007 *Nano Lett* **7** 276-80